Molecular and ionized gas kinematics in the GC Radio Arc

N. Butterfield[1], C.C. Lang[1], E. A. C. Mills[2], D. Ludovici[1], J. Ott[3] and M. R. Morris[4]

[1]Dept. of Physics & Astronomy, University of Iowa, USA
(email: `natalie-butterfield@uiowa.edu`)
[2]Dept. of Physics & Astronomy, San Jose State University, USA
[3]National Radio Astronomy Observatory, USA
[4]Dept. of Physics & Astronomy, University of California, Los Angeles, CA, USA

Abstract. We present NH_3 and H64α+H63α VLA observations of the Radio Arc region, including the M0.20−0.033 and G0.10−0.08 molecular clouds. These observations suggest the two velocity components of M0.20−0.033 are physically connected in the south. Additional ATCA observations suggest this connection is due to an expanding shell in the molecular gas, with the centroid located near the Quintuplet cluster. The G0.10−0.08 molecular cloud has little radio continuum, strong molecular emission, and abundant CH_3OH masers, similar to a nearby molecular cloud with no star formation: M0.25+0.01. These features detected in G0.10−0.08 suggest dense molecular gas with no signs of current star formation.

**Keywords.** Galaxy: center, ISM: clouds, ISM: molecules, masers

1. Introduction

Galactic centre (GC) molecular clouds are suggested to follow 'orbital streams' that are precessing, connected chains of molecular gas (Kruijssen *et al.* 2015). Kruijssen *et al.* (2015, and in this volume) recently proposed an open orbit model that is segmented into four orbital streams. However, modeling these orbital streams is difficult due to several complicated kinematic regions. The complexity of these regions is attributed to multiple streams overlapping along our line of sight (Kruijssen *et al.* 2015; Figure 4).

The Radio Arc: This region has complex kinematics. The molecular cloud at this location, M0.20−0.033 (Serabyn & Guesten 1991), has two velocity components, that are located at 25 & 80 km s^{-1}. Kruijssen *et al.* (2015, and in this volume) argue that these two components to being on the near side (80 km s^{-1}; stream 1) and far side (25 km s^{-1}; stream 3) of the GC. Adjacent to M0.20−0.033 is G0.10−0.08, which is the core of a larger, dense molecular cloud (Tsuboi *et al.* 1997 Handa *et al.* 2006). The orbital model by Kruijssen *et al.* (2015, and in this volume) suggests that this cloud is near pericentre on the near side of the GC (stream 1).

2. Observations

We recently conducted sensitive continuum and spectral line observations with the VLA (NH_3, CH_3OH, H64α and H63α), of M0.20−0.033 and G0.10−0.08, and present the results here. We compare these results with lower resolution ATCA data (NH_3) from Ott *et al.* (in this volume). These observations will be used to analyze the kinematic properties of the molecular gas (as traced by the NH_3 (3,3) transition, hereafter 'molecular gas') and ionized gas (as traced by the combined H64α+H63α transitions, hereafter 'ionized gas').

133
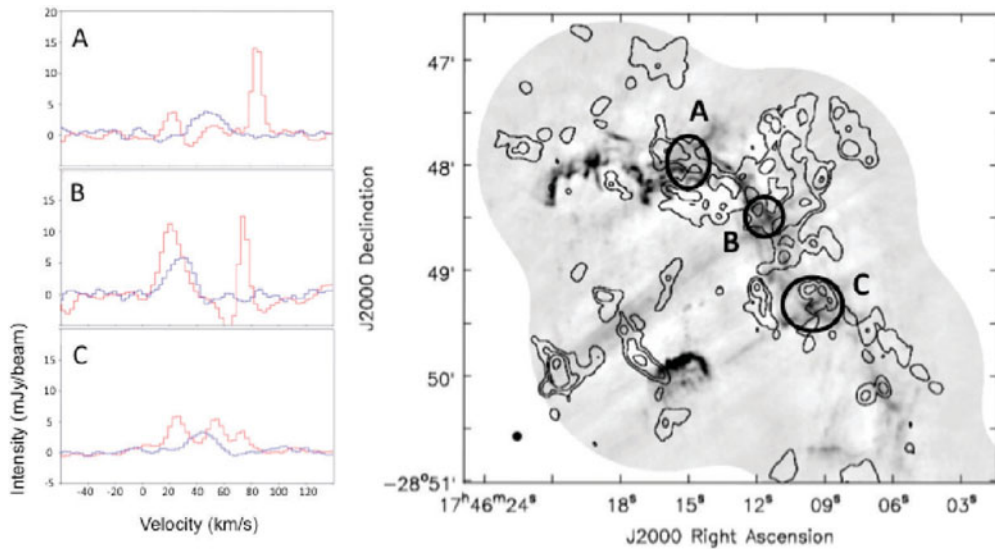
Figure 1. *left*: three spectral panels of NH$_3$ (red; 2−3 components) and H64α+H63α (blue; single component) from the regions (A−C) in (*right*). *right*: 24.5 GHz continuum (greyscale) with contours of NH$_3$ emission at 5, 10, 20, & 50 × 3 mJy beam^{-1} (rms level). The ionized gas emission (not shown) closely follows the continuum emission.

3. Results and Discussion

Connection between ionized and molecular gas in M0.20-0.033: Our VLA observations also show two components in the molecular gas. Figure 1 (right) shows the distribution of molecular gas relative to the 24.5 GHz continuum emission. The spectral distribution of molecular and ionized gas for three selected regions (labeled A−C) are shown in Figure 1 (left). In all three regions, only one ionized gas component is detected. This ionized gas component shows a strong correlation with the 25 km s^{-1} component at position (B). The two northern regions (A & B) show two molecular components separated in velocity space. The most southern region (C) has a third molecular component, located at intermediate velocities ($\sim$50 km s^{-1}). The presence of molecular emission at these intermediate velocities suggests that the 25 & 80 km s^{-1} components in M0.20−0.033 are physically connected in the south via this third velocity component.

Expanding shell in molecular gas: In order to confirm the connection between the two components in the southern region of M0.20−0.033 we examined ATCA data from the SWAG survey. These observations reveal a cavity in the molecular emission that is open on the eastern side (Figure 2). This cavity can be fit with a circle (hereafter, shell; Figure 2), that is centered at R.A.=17$^{\rm h}$46$^{\rm m}$17.3$^{\rm s}$, dec=-28°49$'$00$''$, with a radius r=150$''$($\sim$6pc). An expanding shell produces an elliptical distribution in position-velocity space, because the near side of the shell is blueshifted and the far side of the shell is redshifted. Our position-velocity analysis, using the ATCA data, suggests an expanding shell that has an expansion velocity of $\sim$40 km s^{-1}, with a central velocity of $\sim$51 km s^{-1}. The position-velocity distribution indicates that the 25 km s^{-1} component (blueshifted emission) is on the near side of the shell and the 80 km s^{-1} component (redshifted emission) is on the far side of the shell. H I absorption observations towards this region support such an arrangement (Lang *et al.* 2010). The central velocity of the shell at $\sim$51 km s^{-1} suggests that the shell is located on stream 1 (near side of the GC; Kruijssen *et al.* 2015).
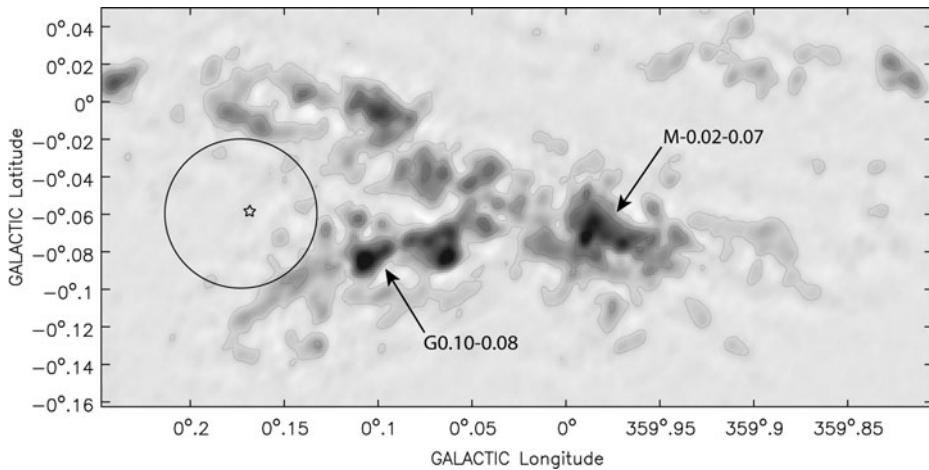
Figure 2. NH_3 (3,3) emission at $50-60$ km s^{-1}, using ATCA observations from the SWAG survey (17″ resolution). The black circle shows the location of our proposed expanding shell. The star denotes the location of the Quintuplet cluster. For more details see Butterfield *et al.* 2016, *in prep.*

Connection to Quintuplet cluster: The massive stellar Quintuplet cluster ($N_{Lyc} \sim 10^{50.9}$ photons s^{-1}, $t_{age} = 4.8 \pm 1.1$ Myr; Figer *et al.* 1999, Schneider *et al.* 2014), is located adjacent to M0.20−0.033. The powerful Quintuplet cluster is capable of ionizing the surrounding ISM, producing the Sickle HII region (Lang *et al.* 1997). The center of the expanding shell is located near (~ 30″ in projection) the Quintuplet cluster (star on Figure 2), suggesting that the shell may be produced by the Quintuplet cluster.

The Kruijssen *et al.* (2015) orbital model suggests that the Quintuplet cluster is located on stream 1. As M0.20−0.033 is also suggested to be located on stream 1, the close proximity of the cluster and cloud indicates a possible interaction, as shown by the Sickle HII region. Since our expanding shell has an estimated age of 1.5×10^5 yr, assuming a constant expansion rate, this suggests that the interaction between the cluster and the cloud is relatively recent.

G0.10−0.08: Another Brick? The VLA observations of G0.10−0.08 indicate that this molecular cloud has several interesting features:

• **Weak Radio Continuum**: G0.10−0.08 has very little radio continuum at 24.5 GHz and no detected ionized gas emission. There is a very faint filamentary streak at 24.5 GHz, near the right edge of the cloud (R.A.=$17^h46^m07^s$, dec=$-28°53'20''$), that is the only emission detected above 5σ. This lack of radio continuum and ionized gas would suggest no embedded star formation in G0.10−0.08. Since there is, however, slight external ionization near the right edge of the cloud, this would suggest ionization from an outside source.

• **Bright NH_3 emission**: The molecular emission in G0.10−0.08 is bright, compared to M0.20−0.033. Figure 3 (greyscale) shows the distribution of the molecular emission, which is abundant throughout the cloud. There are several bright, compact knots of molecular emission distributed throughout G0.10−0.08. The morphology of these compact knots of emission is similar to those detected in M0.25+0.01 (Mills *et al.* 2015).

• **Kinematics**: The molecular gas in G0.10−0.08 ranges from $\sim 30-70$ km s^{-1}, and peaks in intensity at ~ 55 km s^{-1}. The velocity distribution shows a slight gradient (~ 10 km s^{-1} pc^{-1}), in the direction of positive galactic latitude. This gradient is consistent with other GC molecular clouds.
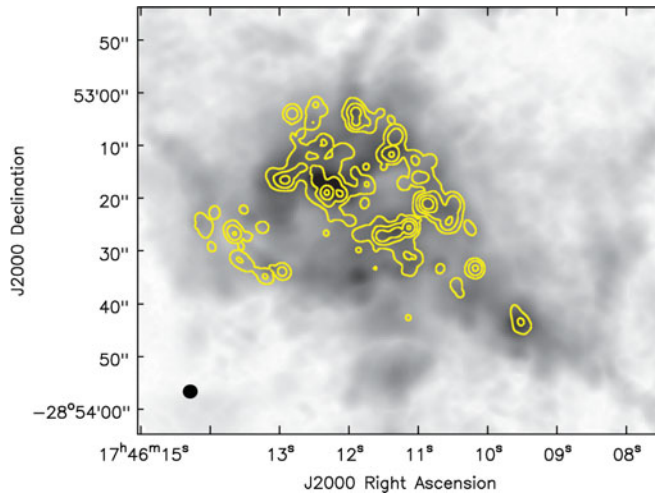
Figure 3. maximum intensity NH$_3$ emission in G0.10−0.08 (greyscale). 36 GHz CH$_3$OH maser contours at 2, 7, 15, and 50 per cent the peak emission (45.7 Jy beam^{-1}).

• **Abundant CH$_3$OH masers**: We have detected 64 compact 36 GHz CH$_3$OH sources (hereafter, CH$_3$OH masers) that have a brightness temperatures above 400 K (Mills *et al.* 2015; Butterfield *et al.* 2016, *in prep*). These CH$_3$OH masers follow the molecular gas emission fairly well (Figure 3). The CH$_3$OH masers in G0.10−0.08 are clustered towards the center of the cloud, where the molecular emission is the strongest. The clustering of CH$_3$OH masers detected in G0.10−0.08 is similar to the 'bar' of masers seen in the southern region of M0.25+0.01 (Mills *et al.* 2015). The 36 GHz CH$_3$OH maser is a class I maser and therefore is a known shock tracer. Thus, the particularly high abundance of CH$_3$OH masers suggest shocked gas towards the core of G0.10−0.08.

Our VLA study suggests that G0.10−0.08 is a dense, compact molecular cloud that shows no signs of current star formation. The molecular characteristics of G0.10−0.08 are similar to those seen in M0.25+0.01 (also known as the 'Brick'; Mills *et al.* 2015). M0.25+0.01 is also suggested to be a quiescent, dense molecular cloud that is not currently forming stars (Longmore *et al.* 2012; Mills *et al.* 2015).

References

Figer, D. F., McLean, I. S., & Morris, M. 1999, *ApJ*, 514, 202
Handa, T., Sakano, M., Naito, S., Hiramatsu, M., & Tsuboi, M. 2006, *ApJ*, 636, 261
Kruijssen, J. M. D., Dale, J. E., & Longmore, S. N. 2015, *MNRAS*, 447, 1059
Lang, C. C., Goss, W. M., & Wood, O. S. 1997, *ApJ*, 474, 275
Lang, C. C., Goss, W. M., Cyganowski, C., & Clubb, K. I. 2010, *ApJS*, 191, 275
Longmore, S. N., Rathborne, J., Bastian, N., *et al.* 2012, *ApJ*, 746, 117
Mills, E. A. C., Butterfield, N., Ludovici, D. A., *et al.* 2015, *ApJ*, 805, 72
Schneider, F. R. N., Izzard, R. G., de Mink, S. E., *et al.* 2014, *ApJ*, 780, 117
Serabyn, E. & Guesten, R. 1991, *A&A*, 242, 376
Tsuboi, M., Ukita, N., & Handa, T. 1997, *ApJ*, 481, 263